Clim Dyn (2013) 41:1651–1669
DOI 10.1007/s00382-013-1854-1

Role of ocean–atmosphere interaction on northward propagation of Indian summer monsoon intra-seasonal oscillations (MISO)

S. Sharmila · P. A. Pillai · S. Joseph · M. Roxy · R. P. M. Krishna · R. Chattopadhyay · S. Abhilash · A. K. Sahai · B. N. Goswami

Received: 13 March 2013 / Accepted: 17 June 2013 / Published online: 12 July 2013

Abstract Atmospheric dynamical mechanisms have been prevalently used to explain the characteristics of the summer monsoon intraseasonal oscillation (MISO), which dictates the wet and dry spells of the monsoon rainfall. Recent studies show that ocean–atmosphere coupling has a vital role in simulating the observed amplitude and relationship between precipitation and sea surface temperature (SST) at the intraseasonal scale. However it is not clear whether this role is simply 'passive' response to the atmospheric forcing alone, or 'active' in modulating the northward propagation of MISO, and also whether the extent to which it modulates is considerably noteworthy. Using coupled NCEP–Climate Forecast System (CFSv2) model and its atmospheric component the Global Forecast System (GFS), we investigate the relative role of the atmospheric dynamics and the ocean–atmosphere coupling in the initiation, maintenance, and northward propagation of MISO. Three numerical simulations are performed including (1) CFSv2 coupled with high frequency interactive SST, the GFS forced with both (2) observed monthly SST (interpolated to daily) and (3) daily SST obtained from the CFSv2 simulations. Both CFSv2 and GFS simulate MISO of slightly higher period (~60 days) than observations (~45 days) and have reasonable seasonal rainfall over India. While MISO simulated by CFSv2 has realistic northward propagation, both the GFS model experiments show standing mode of MISO over India with no northward propagation of convection from the equator. The improvement in northward propagation in CFSv2, therefore, may not be due to improvement of the model physics in the atmospheric component alone. Our analysis indicates that even with the presence of conducive vertical wind shear, the absence of meridional humidity gradient and moistening of the atmosphere column north of convection hinders the northward movement of convection in GFS. This moistening mechanism works only in the presence of an 'active' ocean. In CFSv2, the lead-lag relationship between the atmospheric fluxes, SST and convection are maintained, while such lead-lag is unrealistic in the uncoupled simulations. This leads to the conclusion that high frequent and interactive ocean–atmosphere coupling is a necessary and crucial condition for reproducing the realistic northward propagation of MISO in this particular model.

Keywords Summer monsoon intraseasonal oscillation · Northward propagation · Atmospheric dynamics · Ocean–atmosphere coupling · Climate Forecast System

1 Introduction

The Indian summer monsoon (ISM) is one of the most important land–atmosphere–ocean coupled climate system over the tropics and exhibits substantial variability at seasonal and intraseasonal time scales (Webster et al. 1998). During Boreal summer (June–September, JJAS), the rainfall fluctuations over Indian region are manifested in

This paper is a contribution to the Topical Collection on Climate Forecast System Version 2 (CFSv2). CFSv2 is a coupled global climate model and was implemented by National Centers for Environmental Prediction (NCEP) in seasonal forecasting operations in March 2011. This Topical Collection is coordinated by Jin Huang, Arun Kumar, Jim Kinter and Annarita Mariotti.

S. Sharmila · P. A. Pillai · S. Joseph · M. Roxy · R. P. M. Krishna · R. Chattopadhyay · S. Abhilash · A. K. Sahai (✉) · B. N. Goswami
Indian Institute of Tropical Meteorology, Dr. Homi Bhabha Road, Pashan 411008, Pune, India
e-mail: sahai@tropmet.res.in

the form of active-break cycles intimately associated with the monsoon intraseasonal oscillations (MISO) with horizontal scale much larger than the Indian continent (Sikka and Gadgil 1980; Goswami 2011). The most prominent feature of MISO is the northward propagation of convection and precipitation from equatorial Indian Ocean (EIO) to Indian subcontinent with timescales of 30–60 days (Yasunari 1979, 1980; Sikka and Gadgil 1980; Goswami 2011). Understanding the complex space–time characteristics and propagation mechanism of the MISOs, its realistic simulation and prediction have received considerable attention in recent years (Goswami 2011; Wang 2005; Waliser 2006). Several numerical models, from simple atmospheric to fully coupled ocean–atmosphere general circulation models have been employed to identify the underlying mechanisms of MISOs (Lau and Peng 1987; Wang 1988; Wang and Xie 1997; Fu et al. 2003; Fu and Wang 2004; Waliser et al. 2003, 2004). These quasi-periodic oscillations are considered as the major building blocks of the ISM rainfall as they tend to modulate the synoptic activity on one hand (Goswami et al. 2003) while significantly influencing the interannual variability of the seasonal mean on the other (Goswami et al. 2006). Therefore, correct simulation of space–time characteristics of MISO by a forecast system is crucial not only for the extended range prediction of the active-break spells but also for the long range prediction of seasonal mean monsoon rainfall.

Earlier attempts of simulating ISOs were carried out by atmospheric general circulation models (AGCMs), forced by monthly sea surface temperature (SST) (Slingo et al. 1996; Gadgil and Sajani 1998; Waliser et al. 2003 among others). However, those AGCMs could only simulate rather weak intraseasonal variability, through internal dynamics of the models. Many recent studies have provided compelling evidences indicating that realistic air–sea coupling is crucial in defining and maintaining the observed space–time characteristics of MISO (Krishnamurti et al. 1988; Sengupta et al. 2001; Webster et al. 2002; Vecchi and Harrison 2002; Bhat et al. 2004 among others). Recent studies also emphasize on the importance of ocean–atmosphere interactions in simulating the observed amplitude and the relationship between precipitation and SST at the intraseasonal scale (Wu 2010; Roxy and Tanimoto 2012). Kemball-Cook et al. (2002) compared the ISO produced in the coupled and uncoupled versions of ECHAM4 GCM and showed that ISO could be produced in the uncoupled simulation, although air-sea interaction plays an important role in its organization and intensification. Wu et al. (2002) also suggested that only coupling could adequately depict the time-evolution of the ISO relative to the intraseasonal SST anomalies. Using AGCM coupled with an intermediate ocean model, Fu et al. (2003) showed that ISOs simulated by a coupled model is about 50 % stronger than that simulated by an atmosphere only model forced with monthly varying SST. These results confirm the coupled nature of MISOs since the quadrature phase relationship between atmospheric convection (or precipitation) and SST cannot be simulated by solely using an AGCM with prescribed observed intraseasonal SST. Comparison between the stand-alone and coupled integrations by general circulation models (GCMs) have been made by several researchers (e.g. Kemball-Cook et al. 2002; Fu et al. 2003; Rajendran and Kitoh 2006; Seo et al. 2007; Kim et al. 2011; Rajendran et al. 2012 among others). Most studies emphasize the importance of treating MISOs as a coupled phenomenon and the use of coupled models for better simulation of boreal summer ISOs.

Thus, a coupled ocean–atmosphere model may be essential for extended range prediction of MISO or for seasonal prediction of Indian summer monsoon rainfall. However, realistic simulation of space–time characteristics of MISOs still remains a major challenge for the state-of-the-art climate models (Lin et al. 2006). In addition to errors in simulating the amplitude of MISOs, most models fail to simulate the northward propagation with fidelity (Lin et al. 2006). In the present study, we evaluate the skill of a state-of-the-art coupled model of National Centers for Environmental Prediction (NCEP)–Climate Forecast System model version 2 (CFSv2) and its AGCM, in simulating the MISOs over Indian region. The present study finds that the amplitude and northward propagating characteristics of the MISOs in CFSv2 are more realistic compared to its AGCM. This is noteworthy in light of the poor simulation of northward propagation characteristics of MISO by its earlier version of this model (CFSv1) (Seo et al. 2007; Achuthavarier and Krishnamurthy 2011a, 2011b). Recently Roxy et al. (2012) showed that the upgraded CFSv2 has reasonable SST-precipitation relationship on the intraseasonal scale over tropical monsoon region. In the present study, we show that the improved simulation of MISO in recent version CFSv2 may not be only due to improved physics in the AGCM. It seems that the air-sea coupling itself may resolve this issue in this particular model. By carrying out a series of controlled experiments using CFSv2 and its AGCM, we demonstrate the crucial role of ocean–atmosphere coupling in a realistic simulation of the northward propagating MISOs. Current leading theories on atmospheric dynamic mechanisms prevalently used to explain the northward propagation of MISO (Jiang et al. 2004; Abhik et al. 2013) indicate that atmospheric processes essentially control the northward propagation. If so, what is the relative role of air-sea interaction in the northward propagation of MISO? In the present study, we analyze the results from controlled numerical simulations, and examine the role of air-sea interaction in modifying the

background mean flow and thermodynamics in a way that strongly favors the northward propagation of MISOs.

Section 2 describes the model details and numerical experiments carried out, along with data and methodology. The role of ocean–atmosphere interaction on the MISOs is examined in Sect. 3, and Sect. 4 summarizes the results and discusses their implications.

2 Model, data and methodology

2.1 Model and experimental framework

The most recent version of the NCEP Climate Forecast System model (CFSv2; Saha et al. 2013) is a combination of an atmospheric general circulation model: the Global Forecast System (GFS) model (Moorthi et al. 2001) coupled with the NOAA Geophysical Fluid Dynamics Laboratory (GFDL) Modular Ocean model version 4 (MOM4) (Griffies et al. 2004) with advanced physics, increased resolution and refined initialization than its previous version (CFSv1; Saha et al. 2006) to improve the seasonal climate forecasts. The GFS adopts a spectral triangular truncation of 126 waves (T126) in the horizontal ($\sim$0.9° grid) and a finite differencing in the vertical with 64 sigma-pressure hybrid layers. The convection scheme employed in GFS is the Simplified Arakawa-Schubert (SAS) convection, with cumulus momentum mixing and orographic gravity wave drag (Saha et al. 2010). The ocean component, MOM4 is a finite difference version of the ocean primitive equations configured under the Boussinesq and hydrostatic approximations. The ocean model is coupled with an interactive, 3 layered sea-ice model, an interactive GFDL Sea Ice Simulator. The land surface model (LSM) used in CFSv2 is the Noah LSM, with 4 layers (Ek et al. 2003).

There are three types of numerical simulations examined in this present study (Table 1). First, we examine the MISO simulated in a coupled free run of the CFSv2 integrated for 100 years under fixed CO_2 with air-sea exchange at every half an hour. The initial conditions for the atmosphere and ocean were taken from the NCEP-NCAR reanalysis and NCEP global ocean data assimilation system (GODAS; Behringer and Xue 2004). The last 50 years of the integration are analyzed in the present study and shall be denoted as CFSv2 run. To understand the effect of basic state SST as well as the role of air-sea interactions on simulation of the MISO, two additional integrations were carried out with GFS. To bring out the role of the atmosphere in generating the MISO in the absence of high frequency SST forcing, the atmospheric component of the coupled model (GFS) was forced with observed monthly SST (interpolated to daily) and integrated freely for 60 years. Similarly last 50 years of the free run were analyzed and the results from this experiment are denoted as GFS(m). To delineate the role of the high frequency SST variability in driving the MISO, another run of the GFS was carried out for 50 years forced by CFSv2 simulated daily SST. We shall denote this experiment by GFS(d). We expect that any difference between the simulated MISO from CFSv2 and GFS(d) experiments would just attribute to the impact of air-sea coupling process. All these free simulations with the atmosphere at T126 resolution are performed on Prithvi IBM HPC (High Performance Computing) system at IITM, India. The analyses of the model simulations are compared with the observation to verify their fidelity to reproduce observed reality.

2.2 Observed data

For the CFS/GFS output validation, we use the following high quality and high resolution gridded observational and reanalysis datasets: (a) daily (1° × 1°) global scale precipitation estimates provided by the Global Precipitation Climatology Project (GPCP) (Huffman et al. 2009), (b) daily (1° × 1°) rainfall data from India Meteorological Department (IMD) (Rajeevan et al. 2006), (c) daily gridded data of circulation, vertical pressure velocity, specific humidity at different vertical levels from NCEP-NCAR Reanalysis data (Kalnay et al. 1996), (d) daily fluxes obtained from the TROPFLUX project version 1 (Praveen Kumar et al. 2012) that has a similar performance to the OAFlux product (Yu et al. 2008), (e) daily (0.25° x 0.25°) SST based on the TRMM Microwave Imager (TMI). TMI data are produced by Remote Sensing Systems and sponsored by the NASA Earth Science MEaSUREs DISCOVER Project. The observed fields are referred as OBS in the discussion.

2.3 Methodology

The calculation for the intraseasonal variability is based on 20–100 day band pass filtered (Duchon 1979) daily anomalies computed by subtracting daily smoothed (mean + 1st three harmonics) long term climatology for all the datasets from the observation and the model simulations. These anomalies are referred to as intraseasonal anomalies hereafter.

3 Results and discussions

3.1 Mean state of the Indian summer monsoon

The robustness of any state-of-the-art climate model in simulating reasonable MISOs largely depends on how

Table 1 Details of the coupled and atmosphere only model experiments performed for the present study

Model experiment	Component	SST forcing	Free Integration (years)
CFSv2	Coupled ocean–atmosphere	Initial conditions from NCEP and GODAS	100
GFS(m)	Atmospheric	Monthly observed SST (interpolated to daily)	60
GFS(d)	Atmospheric	Model simulated daily SST	50

realistically it captures the seasonal mean (JJAS) large scale structure of precipitation and atmospheric circulation over the Indian monsoon region. Figure 1a–d compares the model simulated JJAS mean precipitation (shaded) and low level wind (850 hPa; vector) with the corresponding observed precipitation (GPCP) and wind (NCEP-NCAR Reanalysis). It may be noted that CFS simulates the location of the maxima of precipitation quite well together with the northwest-southeast tilt of the rain band. However, it has a dry bias over central Indian region. While the dry bias over central India is significantly improved in GFS(m), it has a strong wet bias over the north Bay of Bengal and the western Ghats. Also it fails to simulate the tilted structure of the rain band. The mean precipitation simulated by the GFS(d) is very similar to that by the CFS. Similar dry bias over Indian land was also noted in the previous coupled version CFSv1 (Chaudhari et al. 2013), and most of the coupled models of this genre have this unresolved problem (Rajeevan and Nanjundiah 2009). The notable discrepancy is that both GFS runs generate spurious double Intertropical convergence zone (ITCZ) instead of a dominant northern ITCZ as in the observation. This may have serious implications in modulating the propagation characteristics of MISOs. The simulation of JJAS mean atmospheric circulation at 850 hPa shows that all the model simulations, especially GFS(m) could simulate realistic mean pattern of low level circulation e.g. the low level cross-equatorial westerlies and cyclonic circulation over the Indian land reasonably (Fig. 1c). However, CFSv2 and GFS(d) produce weaker than the observed circulation over Indian region. In Fig. 2, we also note that, while the seasonal cycle of the precipitation over central Indian region (15°–25°N; 73°–85°E) matches with observations well between August and November in GFS(m) simulations, it precipitates too much in June with the monsoon 'onset' taking place about 2 weeks ahead of observations. The annual cycle also shows significant dry bias over the continental India during the monsoon season simulated by CFSv2 and the GFS(d). The difference in JJAS rainfall and circulation pattern between the coupled run and the stand-alone runs indicates

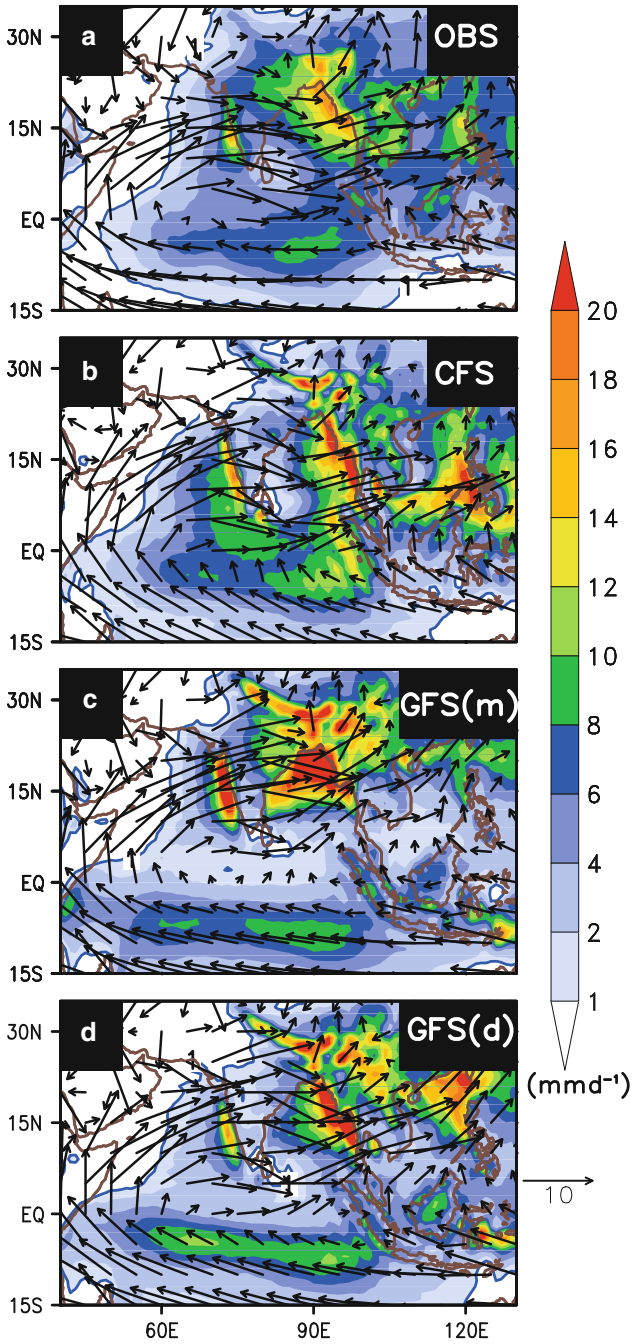

Fig. 1 Seasonal (JJAS) mean precipitation (mm day^{-1}, shaded) and low level (850 hPa) circulation (ms^{-1}, vector) for **a** OBS (GPCP), **b** CFS, **c** GFS(m) (*forced with observed monthly SST daily interpolated*), **d** GFS(d) (*forced with model simulated daily SST*)

that the tropical air–sea interactions considerably change the ISM climatology and is necessary for a more realistic simulation over the ISM domain. However, weaker monsoon and low precipitation over land in CFSv2 and GFS(d) may be attributed to the considerable cold SST bias of about 2–3 °C in the CFSv2 over the tropical ocean (Roxy and Tanimoto 2012; Roxy et al. 2012) as well as the

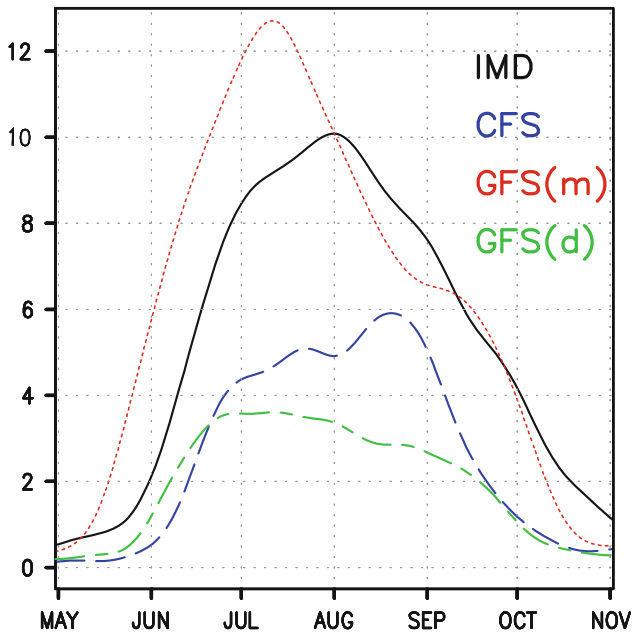

Fig. 2 Seasonal cycle of precipitation over central Indian region (73°–85°E; 15°–25°N) as simulated by CFS (*blue dash*), GFS(m) (*red dot*) and GFS (d) (*green dash*) compared to OBS (IMD; *black solid*)

remarkably colder Tropospheric temperature over the Asian continents (figure not shown).

3.2 Simulation of MISOs

3.2.1 Intraseasonal variability (ISV)

The percentage (%) variances of ISV (shaded) to the total daily variance (contour) in JJAS are shown in Fig. 3a–d. In the OBS (Fig. 3a), the 20–100 day mode of ISV variance explains about 20 % of the total daily variance over the Indo-Pacific monsoon domain (similar to Goswami 1998), while in the GFS and CFSv2 simulations it contributes to more than 25 %. Previous studies indicate that there are primarily five regions of high amplitude intraseasonal variability (ISV) activity over the extended Indian monsoon region, namely; over the eastern Arabian Sea, Bay of Bengal, South China Sea, the western-north Pacific and the equatorial Indian Ocean (Fu and Wang 2004). It is found that CFSv2 is in good agreement with OBS and captures the overall observed pattern, though it overestimates the amplitudes over western Arabian Sea. It may be noted that the total daily variance simulated by the CFSv2, GFS(m) as well as GFS(d) is comparable, albeit a little stronger than the observed daily variance (Fig. 3). The percentage of daily variance explained by MISO, however, is higher in CFSv2 (Fig. 3b) compared to observations (Fig. 3a) with the model producing excess MISO variance in the western Arabian Sea and in South China Sea. It is seen from GFS(m) simulations (Fig. 3c) that these biases are inherent in the atmospheric component of the model and is slightly enhanced by the air sea coupling. It is also of interest to note that the GFS(m) version itself produce enough ISO variance during Boreal summer and air-sea coupling is not required to enhance the amplitude of MISO in the CFSv2 to the observed level.

3.2.2 Wavenumber—frequency spectra of precipitation

The most significant character of MISO is the pronounced 30–60 day oscillations of northward propagating convection anomalies over ISM domain. Therefore, the meridional (north–south) wavenumber frequency spectrum analysis is carried out over the ISM domain (65°–90°E; 15°S–30°N) during boreal summer (May–October) to identify how well the coupled and uncoupled models simulate such a dominant mode compared to the observations, following the methodology of Wheeler and Kiladis (1999) and Joseph et al. (2012). The signal-to-noise-ratio of precipitation is computed by dividing the raw power in precipitation by an estimate of its red noise background. The background spectrum is estimated by smoothing the power repetitively using a 1-2-1 filter until saturation. Figure 4a–d shows the summertime north–south space–time spectra of daily precipitation from GPCP and the model simulated daily precipitation from CFSv2, GFS(m) and GFS(d). A dominant northward propagating mode of 30–60 day period and wavenumber 1 with maximum power at 45 days is noted in GPCP (Fig. 4a). Comparing the model simulated spectrum to that of observations, it appears that all three runs could give ISO signal at wavenumber 1 but slightly at a longer period. It may also be noted that the magnitude of the power is quite weak in GFS(m) (Fig. 4c) as compared to CFSv2 (Fig. 4b) and GFS(d) (Fig. 4d). It seems that GFS without intraseasonally varying observed SST could simulate the ISO signal in some way, but unable to simulate the magnitude and the periodicity correctly. To verify the correct fraction of meridionally propagating MISOs, we estimate the ratio of northward and southward power of the precipitation spectrum averaged over 30–90 day period (Fig. 5). It is noted that although CFSv2 overestimates the ratio at wavenumber 2, it reproduces the ratio close to OBS at wavenumber 1, while GFS(d) shows the northward magnitude relatively smaller at the same wavenumber. However, GFS(m) has failed to simulate the correct ratio as expected. It is suggested here that realistic simulation of MISO depends on how well a model captures the northward and southward power as compared to OBS and ocean–atmosphere coupling seems to be crucial for it.

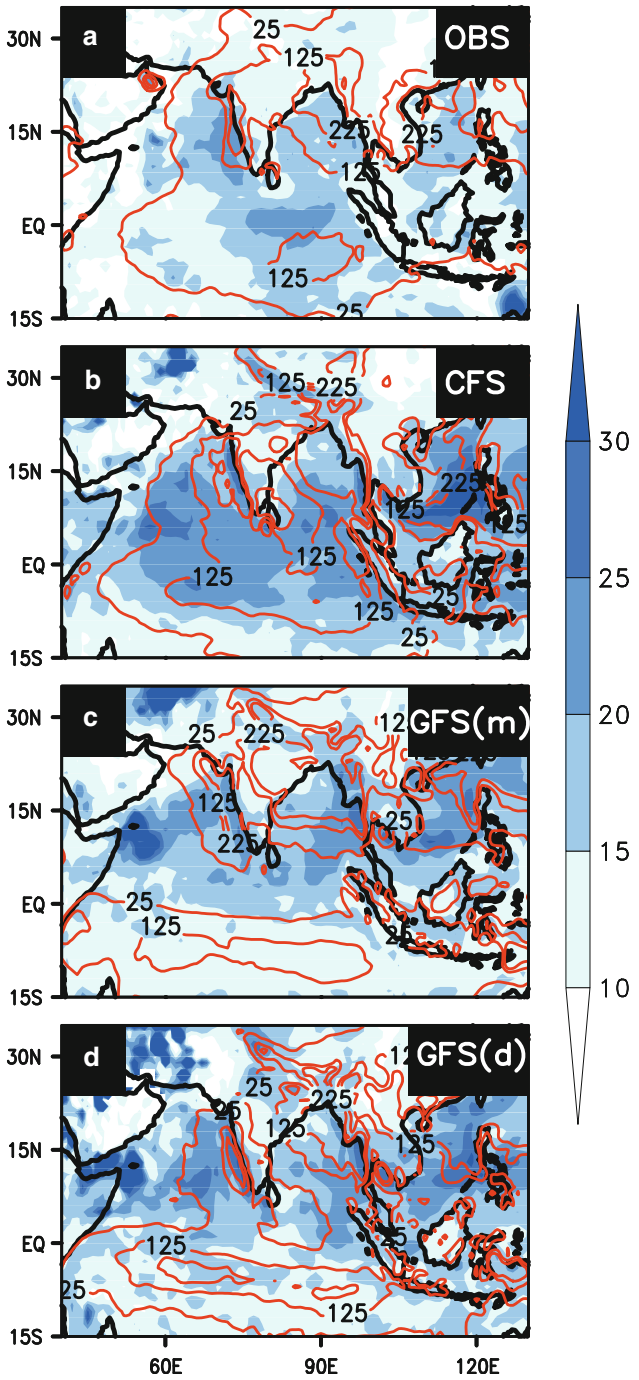

Fig. 3 The percentage variance explained by the 20–100 day filtered precipitation(*shaded*) to the total daily variance ($mm^2\ day^{-2}$; *red contour*) during summer monsoon for **a** OBS, **b** CFS, **c** GFS(m) and **d** GFS(d) respectively

3.2.3 *Space–time evolution of northward propagating MISOs*

To examine the life cycle of the northward propagating MISO, the 20–100 day filtered precipitation anomalies are regressed at different time lags with respect to a reference time series based on the filtered precipitation anomalies area-averaged over monsoon trough region (15°–25°N, 70°–90°E) normalized by its standard deviation during JJAS. Figure 6 shows the time-evolution of the regressed precipitation anomalies of MISOs from day −20 to +10 days for OBS (GPCP), CFSv2, GFS(m) and GFS(d). Here, day 0 is the day of rainfall maxima over the core region of central India. OBS (Fig. 6a) shows that the convection first initiates over the western Indian Ocean around day −20, and with successive days it extends eastward (day −15) and then moves northwestward to Indian subcontinent by day −5. Around day 0, the MISO has a quadruple structure with eastward tilted rain band over Indian region extended up to the maritime continent, and suppressed convection over EIO and north Western Pacific (Annamalai and Slingo 2001). Subsequently, the positive rainfall anomalies further move to the foothills of the Himalaya (∼day 10) followed by negative rainfall anomalies from EIO. It is evident from the simulations that, from the initiation of the ISO convection over the equatorial Indian Ocean (EIO) to the northward propagation in the successive days, the CFSv2 (Fig. 6b) has well captured the life-cycle of the MISOs, as compared to OBS. However, the atmosphere-only GFS(m) has no such organized convection over the EIO. Thus there is reduced convection over the Indian subcontinent and increased convection over South China Sea region up to day −10. The pattern reverses by day −5 and at day 0 there is increased convection over India and reduced one over north Western Pacific and east Indian Ocean. Therefore GFS(m) failed to simulate the observed lifecycle of MISO. At the same time, with daily model SST, GFS(d) shows marginal improvement in organization of convection over eastern EIO in day −20 and it moves northward to central Indian region by day 0. However, we note that at day 0, the northwest-southeast tilted large scale structure of MISO is largely missing in GFS(d), similar to that simulated by GFS(m). Thus the space–time evolution of MISO indicates that CFSv2 exhibits fairly good agreement with OBS, while GFS(m) lacks the evolution and GFS(d) shows little resemblance to CFSv2. Figure 7 is the hovmöller diagram of regressed rainfall anomalies averaged over the Indian longitudes 70°–90°E for OBS and the model simulations. In CFSv2, the northward propagation of the convection anomalies from equatorial region to core monsoon region is in good agreement with OBS, though having longer period compared to OBS. However, GFS(m) exhibits no propagation of convection anomalies from EIO, and only standing oscillation of convection over the Indian subcontinents. Meanwhile, GFS(d) simulates slight northward pattern especially north of 5°N compared to GFS(m).

The above analysis brings out the fact that MISO simulated by coupled CFSv2 has realistic spatial pattern and

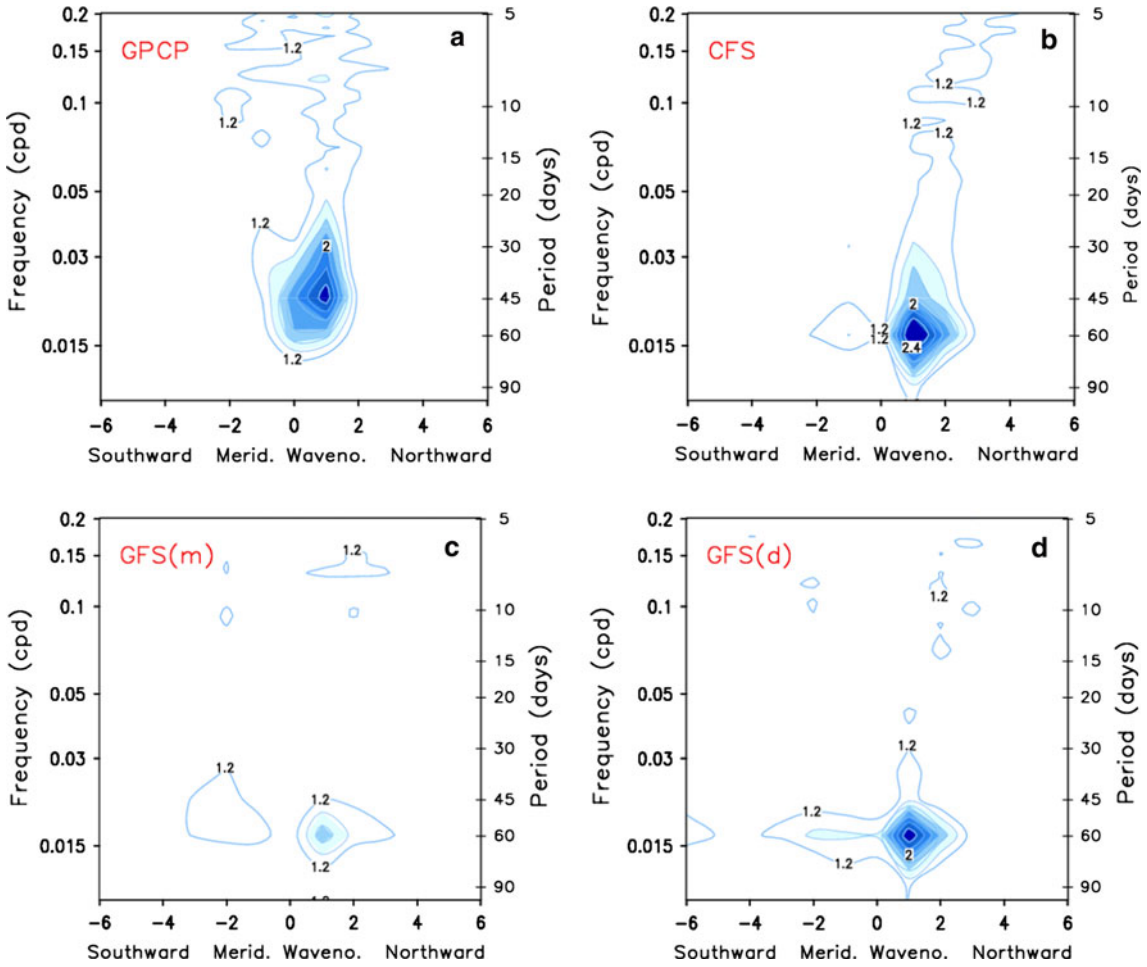

Fig. 4 Boreal summertime meridional wavenumber-frequency spectra of precipitation over 15°S–30°N and 60°–95°E domain for **a** OBS (GPCP), **b** CFS, **c** GFS(m), **d** GFS(d) simulations. *Shading* is from 1.4 with contour intervals of 0.2

northward propagation, while both the atmospheric models GFS(m) and GFS(d) were unsuccessful in simulating the northward propagation of MISO, although GFS(m) simulates the rainfall seasonal cycle well over central Indian region. Now, a question arises here: what is responsible for the presence (or absence) of northward propagation of MISO in the models? Previous studies on underlying mechanisms of northward propagating ISOs advocate the role of the atmospheric internal dynamics (Webster 1983; Goswami and Shukla 1984; Wang and Xie 1997; Jiang et al. 2004, 2011; Bellon and Sobel 2008; Abhik et al. 2013) and also emphasize on the impact of atmosphere–ocean coupling in simulating the improved MISO in models (Kemball-Cook and Wang 2001; Fu et al. 2003, 2008; Xavier et al. 2008). Analyzing the space–time character of MISO in CFSv2 and its atmospheric models, we believe that the air-sea coupling other than the atmospheric internal dynamics of the model plays the key role in driving the MISO northward in CFSv2. To establish this fact, we first examine the important atmospheric processes in the models in the next section followed by the analysis of the coupled processes.

3.3 Atmospheric connections on northward propagation of MISOs

3.3.1 Hadley and Walker circulation

The analysis in the previous sections showed that GFS runs were unable to simulate the mean JJAS precipitation from equator to 10°N (Fig. 1c, d) and also failed in reproducing the movement of convection from equator to monsoon region (Fig. 6). This leads us to the speculation that there is major problem in the simulation of seasonal mean heat source in the equatorial Indian Ocean and its interaction with regional and planetary scale circulations. The ISM may be viewed as a superposition and interaction between a regional Hadley circulation and a planetary-scale Walker circulation. The seasonal mean Walker circulation may be influenced by the movement of the equatorial heat sources,

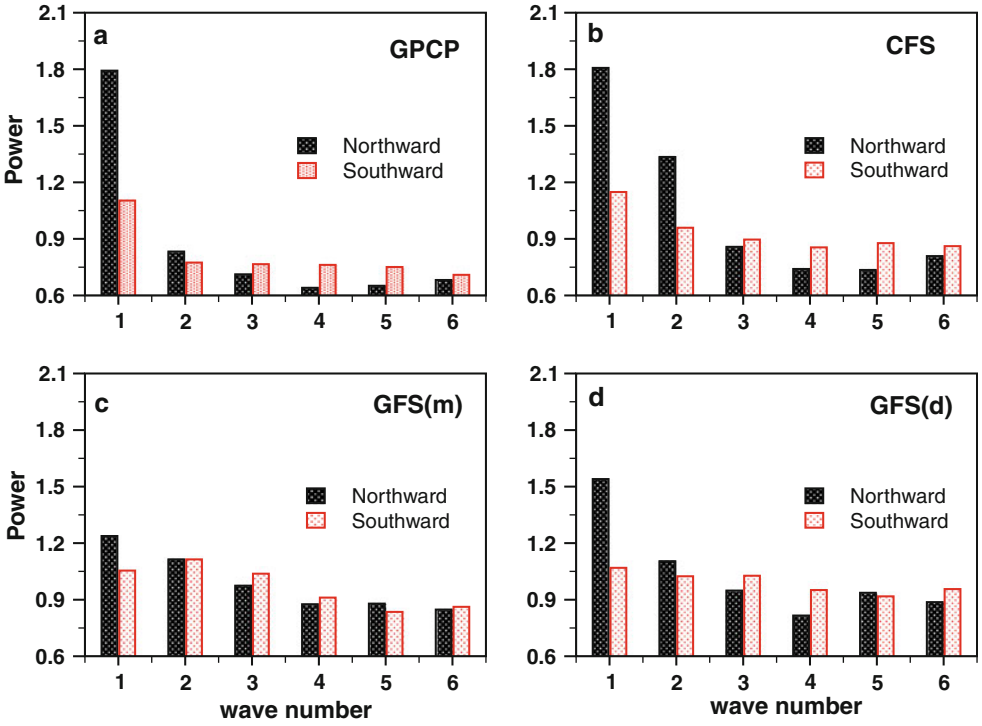

Fig. 5 Power of precipitation spectrum separated as northward and southward components (calculated from meridional-wavenumber frequency spectra of precipitation) averaged over the period 30–90 days for **a** GPCP, **b** CFS, **c** GFS(m) and **d** GFS(d)

while the seasonal mean regional Hadley circulation may be affected by the strength and location of the monsoon heat sources (Goswami et al. 1999) during boreal summer. Therefore, both the atmospheric circulations associated with the heat sources may strongly affect the distribution of seasonal mean precipitation during ISM. To address this issue, we examine the simulated JJAS regional Hadley circulation (Fig. 8; averaged over 70°E–90°E) and the Walker circulation (averaged over 10°S–10°N; Fig. 9) for CFSv2, GFS(m) and GFS(d), in comparison with the observation. Figure 8 shows that all coupled and uncoupled models could simulate one ascending branch over Indian subcontinent and another south of the equator, and are in agreement with the precipitation pattern in Fig. 1. It is interesting to note here that GFS(m) and even GFS(d) forced with daily model SST simulate strong subsidence over the equator up to ~10°N, the region of unrealistically low JJAS precipitation. Such erroneous subsidence may interrupt the northward migration of the equatorial convection. However, with air-sea coupling, CFSv2 counteracts the subsidence, and better simulates the overall Hadley circulation with overestimation in the ascending branch over off-equatorial region compared to OBS. Similar to Hadley circulation, CFSv2 shows significant improvement in simulating the seasonal Walker circulation as compared to GFS(m) and GFS(d) (Fig. 9). Both the GFS simulations show strong low level descending motion over the equatorial Indian Ocean region from the equatorial western Pacific region, thus largely underestimate the zonal variability in the near-equatorial rainfall as well as the lower Tropospheric convergence zone. These results imply that, even with high frequency SST forcing, AGCM is unable to reproduce the monsoon heat sources and associated atmospheric circulations realistically, while air-sea coupling could reasonably improve the location, movement and the strength of such heat sources.

3.3.2 Atmospheric internal dynamics

Previous studies point out that the atmospheric internal dynamics along with the vertical easterly shear of the mean flow and meridional asymmetry in specific humidity are the essential factors for the northward propagation of MISOs (Jiang et al. 2004; Drbohlav and Wang 2005). Some studies also suggest that an AGCM is sufficient to simulate northward propagation of MISOs from the atmospheric internal dynamics, and that coupling may further improve it close to observation (Jiang et al. 2004). Figure 10 shows the JJAS mean meridional variation of the vertical easterly shear (U_{200}–U_{850}; ms^{-1}; Fig. 10a), the specific humidity (q, g kg^{-1}; Fig. 10b) at 1,000 hPa, and the respective rainfall (Fig. 10c) averaged over the longitudinal domain of 70°–90°E for the GFS(m), GFS(d) and CFSv2 compared to OBS. It is evident that both the GFS runs simulate the meridional variation of the vertical easterly shear more realistically than CFSv2. CFSv2. From Fig. 10b, it seems that the magnitude of the surface specific humidity over land region (~20°N) is better simulated in GFS(m) compared to CFSv2 and GFS(d). However, the meridional

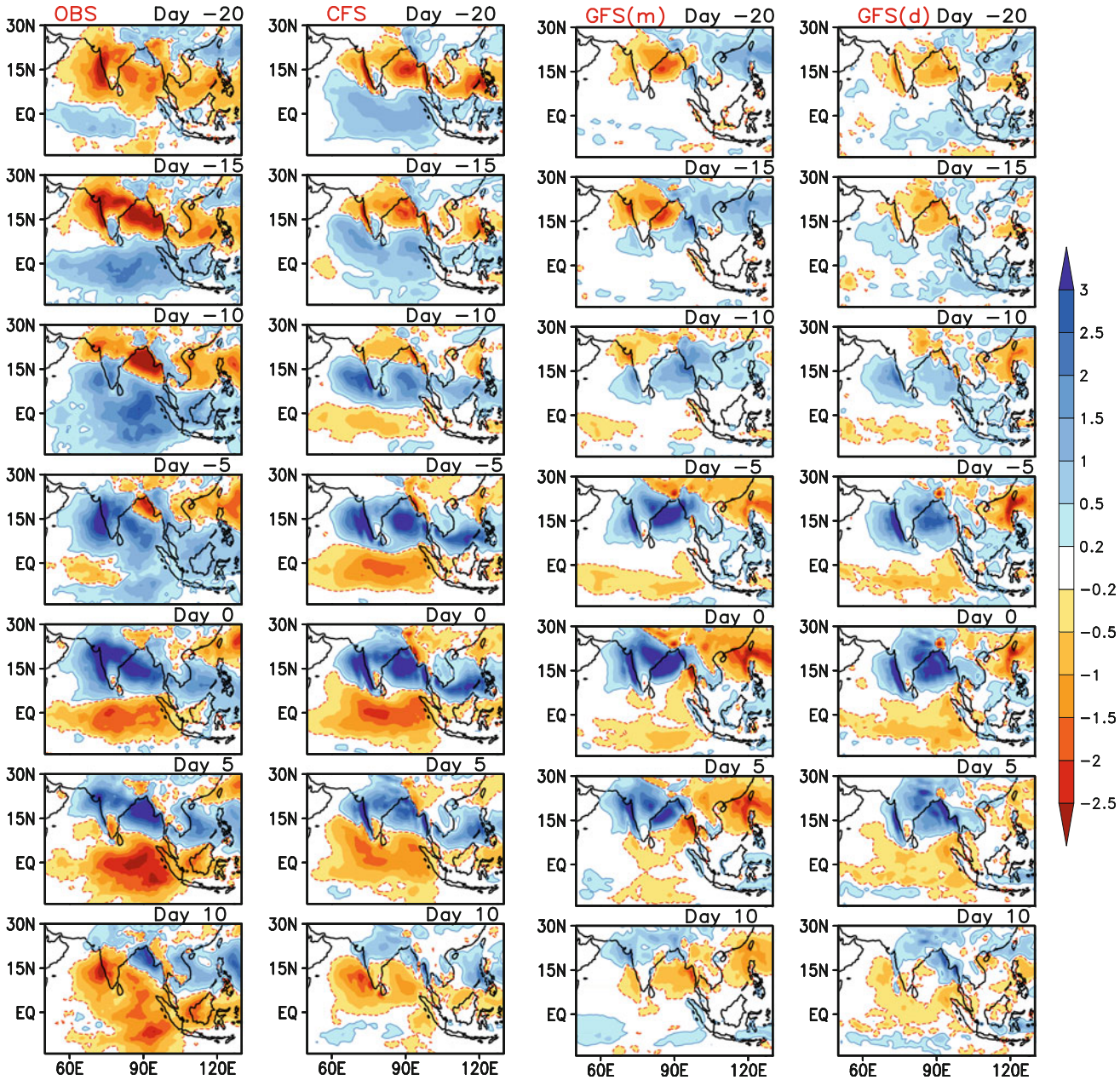

Fig. 6 Space-time evolution of the regressed 20–100 day filtered precipitation anomalies from day −20 to day +10 over monsoon region with respect to a reference time series area averaged over central Indian region for the OBS (GPCP; 1st panel), CFS (2nd panel), GFS(m) (*forced with observed monthly SST daily interpolated*; 3rd panel) and GFS(d) (*forced with model daily SST*; 4th panel) respectively. Here day 0 is the day of rainfall maxima

gradient (from oceanic region to land) of specific humidity in GFS(m) is sufficiently weak compared to CFSv2 and GFS(d) (Fig. 10b), which is essential for northward propagation of MISO (Jiang et al. 2004). The insufficient meridional gradient of specific humidity in GFS(m) may thus cause inbuilt subsequent increase in the rainfall over the land region (refer Fig. 2). This may also probably be linked to the misrepresentation of the seasonal mean precipitation (Fig. 1c) and lack of northward propagation of MISO in GFS(m). In both CFSv2 and GFS(d), the decrease in the magnitude of surface specific humidity over land region probably related to the seasonal mean dry bias in precipitation over land region (Fig. 1b, d). However, it is very intriguing fact that the GFS(d), which has comparable vertical shear and meridional gradient of moisture, has large discrepancy in the northward propagation of MISO (refer Figs. 6, 7c). Therefore, the fundamental mechanisms on northward propagation of MISOs that represent the role

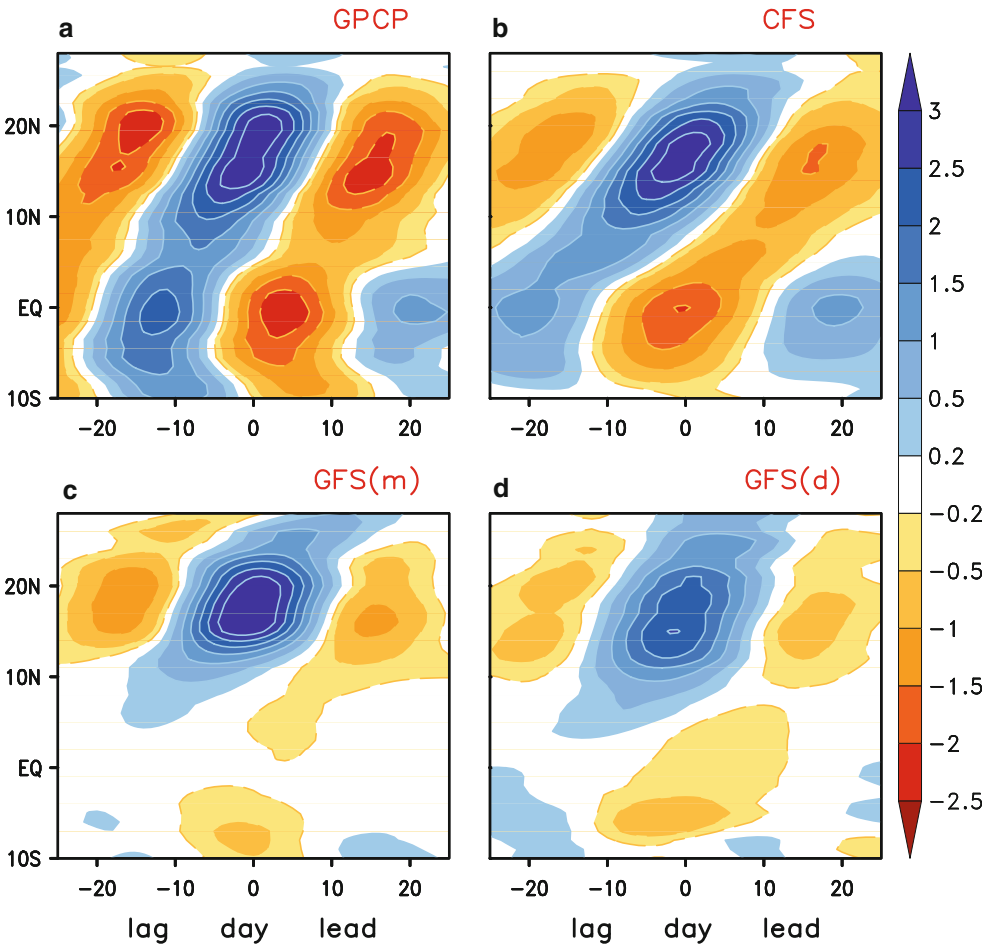

Fig. 7 Hovmöller plots of regressed 20–100 day filtered precipitation anomalies averaged over 70°–90°E with respect to a reference time series area averaged over central Indian region for the **a** GPCP, **b** CFS, **c** GFS(m) and **d** GFS(d) respectively. Here day 0 is the day of rainfall maxima

of atmospheric internal dynamics need to be studied in detail here.

Jiang et al. (2004) proposed that the combination of *vertical wind-shear mechanism* and *moisture convection feedback mechanism* are essential for the northward propagation of the MISO convection. Using an AGCM, they demonstrate that the northward shift of enhanced lower level moisture convergence along with a positive equivalent barotropic vorticity perturbation help in preconditioning the lower atmosphere for the northward propagation of MISO convection. Moreover, many other studies also identify the possible role of the heat fluxes, moisture and moist static energy (MSE) in the poleward propagation of ISOs (Webster 1983; Wang and Xie 1997; Kemball-Cook and Wang 2001; Prasanna and Annamalai 2012, among others). Prasanna and Annamalai (2012) suggested that the destabilization associated with the ISO is brought about by a combination of a low-level build up of MSE and drying of the middle atmosphere due to subsidence from the wake of a previous ISO event. Further, Roxy and Tanimoto (2007, 2012) indicated that ocean-atmospheric processes during an active phase of the ISO induce positive MSE anomalies, which destabilize the lower atmospheric column and enhance the ISO convective activity. Therefore, we analyze the simulated meridional asymmetry of dynamic and thermodynamic fields with respect to the MISO convection to further verify the proposed mechanisms for both the GFS and CFSv2. The formulation of moisture budget and MSE budget are summarized in Appendix. Figure 11a–c shows composite meridional profile of rainfall (*black line*) and associated low level vorticity (850 hPa; *red line*), omega at 500 hPa (−ve value; *green line*), and surface latent heat flux (LHF; *blue line*) averaged over 70–90°E with respect to ISO convection maxima based at selected locations (e.g. EIO and Indian subcontinent) for CFSv2, GFS(m) and GFS(d) respectively. Here, the horizontal axis represents the meridional distance with respect to maximum convection centre denoted as '0' and positive (negative) value means the degrees to the north (south). It is evident from Fig. 11a that in CFSv2, the low level positive vorticity and surface LHF is ∼3° shifted to the north of the convection, with omega at 1° ahead. Therefore, the dynamical parameters help in the development of convective heating to the north of the existing convection and favor northward movement of convection in CFSv2. In contrast, it is noted that the low level positive vorticity and vertical velocity coincides with convection

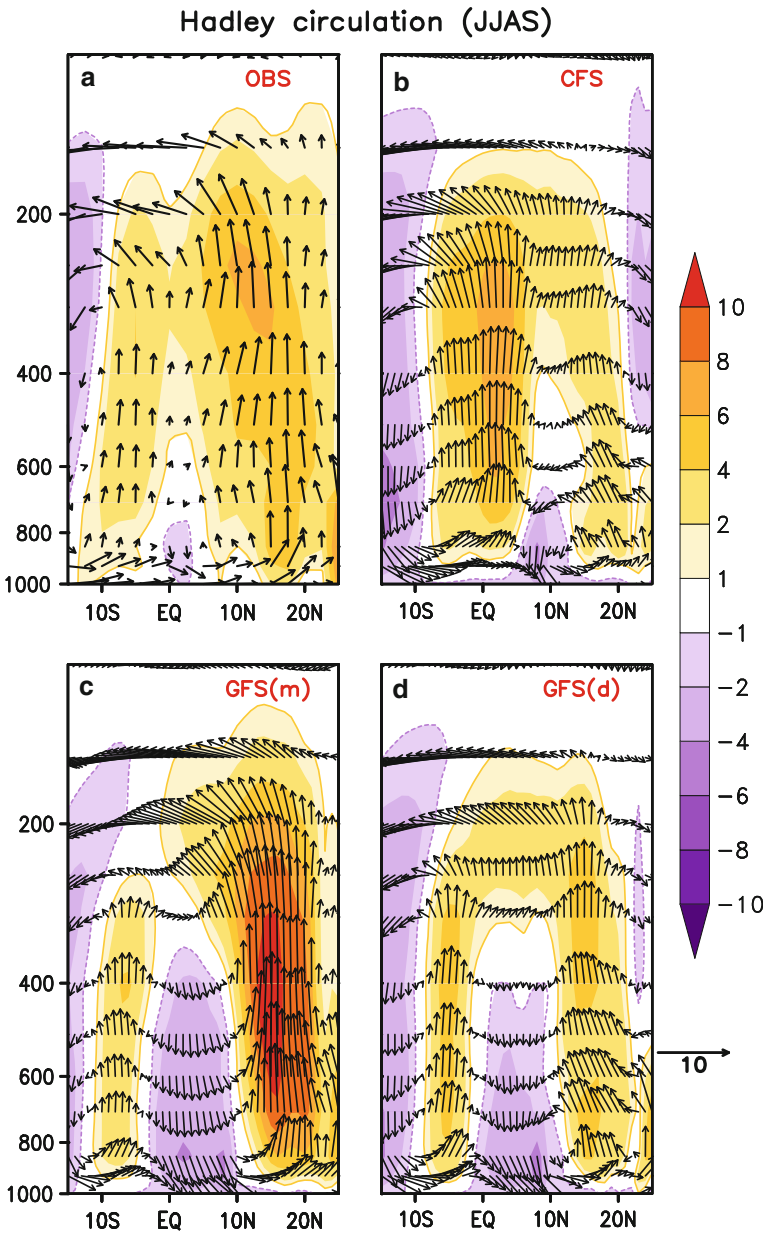

Fig. 8 Seasonal (JJAS) mean Hadley circulation averaged over 70°–90°E for **a** OBS, **b** CFS, **c** GFS(m) and **d** GFS(d) simulations. Here omega is multiplied by -1×100. Unit: omega (ω: Pa s^{-1}); meridional wind (v: ms^{-1})

centre in GFS(m) (Fig. 11b); also the surface LHF maxima is 2° south of convection centre. Therefore, it does not support the proposed theory, even though strong vertical easterly shear is present in GFS(m). However, in GFS(d) only the low level positive vorticity leads convection by 2°, while the mid level omega coincides with the convection. Further, the surface LHF maximum is also to the south of the convection indicating the role of wind in controlling LHF. This indicates that although the change in the high frequency SST forcing has improved the vorticity propagation in the AGCM simulation; it is still not sufficient to shift the MISO convection northward.

In a similar way, we also attempt to demonstrate whether the convection-moisture feedback mechanism really holds well in the GFS simulations and in CFSv2 or not. Figure 11d-f shows the composite meridional profile of rainfall, surface humidity, meridional advection and vertical advection of humidity and also MSE divergence with respect to convection centre for CFSv2, GFS(m) and GFS(d) respectively. Positive MSE anomalies indicate upward motion of moist air associated with moisture convergence at the lower level, and divergence of dry air at the upper level. Such conditions will favor the shifting of the specific humidity to the north of the convection and thus favor the northward propagation of convection. In CFSv2 (Fig. 11d), all these parameters have maximum positive value north of the convection centre indicating that moisture advances ahead of convection and the atmospheric column ahead of convection is also

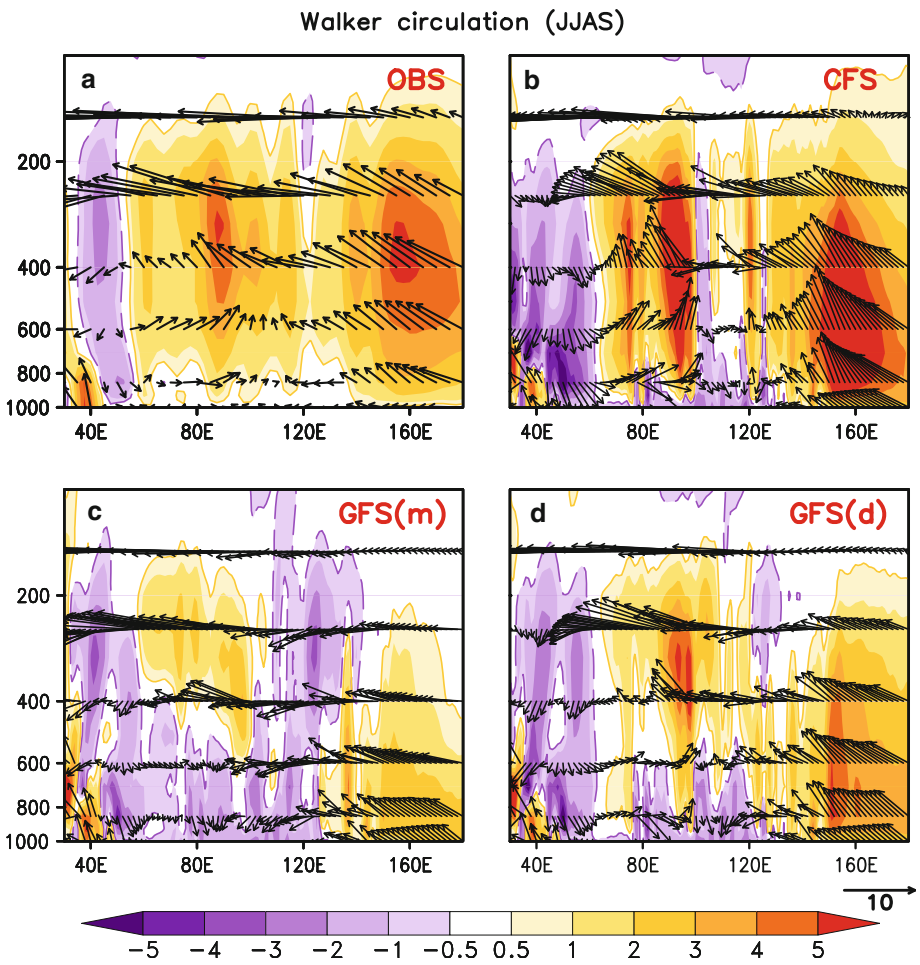

Fig. 9 Seasonal (JJAS) mean Walker circulation averaged over 10°S–10°N for **a** OBS, **b** CFS, **c** GFS(m) and **d** GFS(d) simulations. Here omega is multiplied by -1×100. Unit: omega (ω: Pa s^{-1}); zonal wind (u: ms^{-1})

moistened before convection. Meanwhile, in the GFS(m) (Fig. 11e), all these parameters, except surface specific humidity (that coincides with convection centre), have maximum value south of convection maxima, indicating that the convection itself moistens the atmosphere. However, in GFS(d) (Fig. 11f), horizontal advection of moisture and surface humidity advances ahead of precipitation, but vertical movement of moisture and MSE are collocated with the convection maxima, indicating that convection itself moistens the atmosphere.

These results indicate that both the mechanisms for northward propagation of MISO fails in the case of GFS(m), implying that even in the presence of strong easterly vertical shear, the absence of accurate representation of moisture field hinders the northward propagation of MISO. However, forced with intraseasonal SST, GFS(d) shows a little but not sufficient improvement in this regard. In the climatological picture itself, we notice a subsidence zone from equator to 10°N (Fig. 8, Hadley circulation), which can induce dry air advection in the entire atmosphere hindering the vertical motion of moist air in the GFS(m). The subsidence in the equator-10°N zone is reduced in the GFS(d), but is still present, which may obstruct the buildup of atmosphere column moisture before the precipitation in the AGCMs. However, high frequency SST coupling in CFSv2 has overcome such inherent bias in the AGCM and improves the atmospheric internal dynamics, leading to well organized northward propagation of MISOs. Therefore, the above results indicate the important role of air-sea coupling in driving the northward propagation of MISOs in the CFSv2 model. Due to the lack of spatial structure and variability in simulating MISOs, GFS(m) is eliminated from further analysis.

3.4 Role of air-sea interaction in the northward propagation of MISOs

Earlier studies indicate that the air-sea interaction plays an imperative role in maintaining the observed MISO. While many AGCM simulations with monthly varying SST are able to produce some ISV, interactive air-sea coupling is required for realistic simulation of periodicity, intensity as well as the phase relationship between SST and precipitation close to observation (Wu et al. 2008). In this subsection, we demonstrate how important is the ocean–atmosphere coupling for the realistic simulation of MISO and its characteristics. We compared the results from

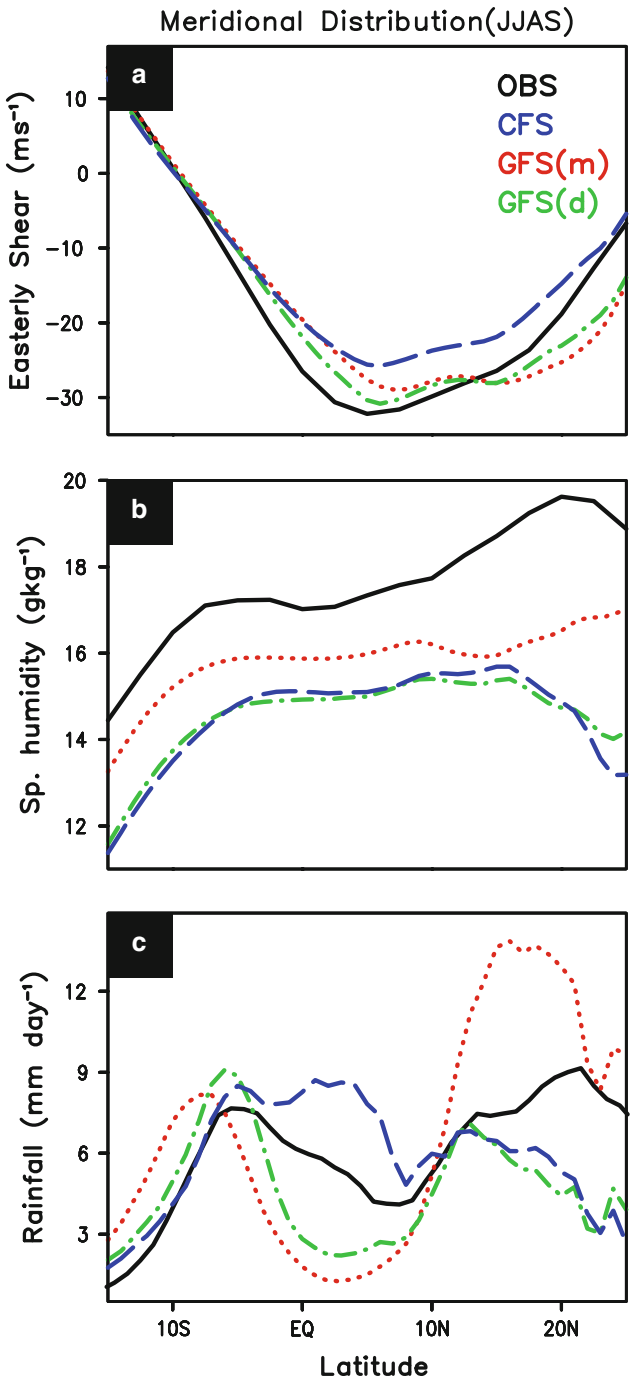

Fig. 10 Seasonal (JJAS) mean meridional distribution of the **a** vertical shear (U_{200}–U_{850}; ms^{-1}), **b** specific humidity ($g\ kg^{-1}$) at 1,000 hPa, and **c** rainfall ($mm\ day^{-1}$) averaged over the longitudinal band 70°–90°E for CFS (*blue dash curve*), GFS(m) (*red dot curve*) and GFS(d) (*green dash curve*) simulations compared with OBS (*black solid curve*)

CFSv2 and GFS(d) with same basic states in order to isolate the impact from just the coupling.

Recent work by Roxy et al. (2012) compared the SST-precipitation mechanism of CFSv2 with observation. They found that ocean–atmosphere coupling is well simulated in the model, but with an overestimation leading to a stronger SST-precipitation relationship. Besides, the accurate lead-lag relationship of convection with surface dynamics and thermodynamics is also vital for the northward propagation of MISOs (Prasanna and Annamalai 2012, among others). To understand the relative role of the interactive SST on the northward propagation of MISOs, we investigate the lead-lag relationship between the ocean and atmospheric parameters (SST, fluxes and precipitation) at ISO timescale. We select the Bay of Bengal (BoB) where strong ISO signal is prevalent (Sengupta et al. 2001; Roxy et al. 2012). Strong ISO events based on a 5° × 5° box were identified over the BoB region (15°–20°N; 87°–92°E) in order to better characterize the possible active role of air-sea coupling in driving the northward propagation of MISOs. Figure 12 shows the Hovmuller diagrams of 20–100 day filtered intraseasonal anomalies over BoB averaged over 85°–95°E for OBS, CFSv2 and GFS(d) (in each column respectively) to identify the lead-lag relationship among the surface dynamical and thermo-dynamical variables that largely control the northward propagation of MISOs. Here day 0 is the day of precipitation maxima over that box. In Fig. 12a, it is noted that in CFSv2, the positive SST anomalies (contour) leads the precipitation anomalies (shaded) by 8–9 days over BoB, close to the OBS (GPCP and TMI-SST) and consistent with the earlier studies (Vecchi and Harrison 2002; Roxy and Tanimoto 2007, 2012). However, the SST maxima is seen nearly in phase with rainfall in GFS(d) giving little southward shift. Since the observed response of precipitation to SST anomalies at BoB occurs over a period of 8–9 days, an instantaneous response in the GFS(d) model simulation means that the atmospheric response to the ocean is not captured realistically. The ISO driven atmospheric net heat flux variations also impart intraseasonal signals on SST. To examine this fact, the lead-lag relationship between the interactive SST and the net heat flux is also examined. The net heat flux at the surface (Q_{net}) is the product of surface downward short wave radiation (SWR), upward long wave radiation (LWR) and latent heat flux (LHF) and sensible heat flux (SHF). While Q_{net} leads SST by ~5 days in CFSv2 similar to OBS, it is collocated with SST in GFS(d) with standing behaviour (Fig. 12b). Similarly, other fluxes and surface zonal wind anomalies (U_{1000}) are examined at the ISO scales with respect to the precipitation maxima. It is noted that LHF and SWR are collocated with Q_{net} in all the cases (Fig. 12c), reflecting their in phase relationship with Q_{net}. Meanwhile in GFS(d), the larger reduction in SWR over the convection maxima signifies that the region is cloudier in GFS(d) compared to CFSv2. We also note that in CFSv2, the surface easterly anomaly develops prior the precipitation maximizes at day 0 as in the OBS (Fig. 12d). It tends to enhance the downward latent heat flux (Fig. 12f)

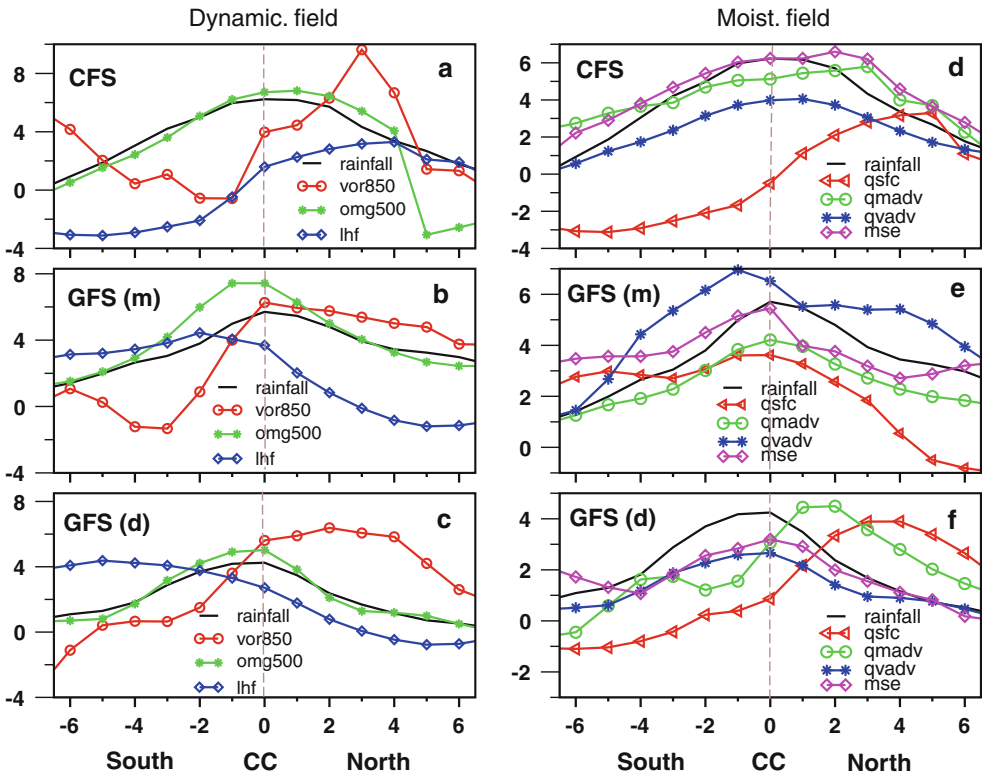

Fig. 11 Meridional profiles of anomalous dynamical and moisture parameters for CFS, GFS(m) and GFS(d) with respect to rainfall maxima (convection centre; CC) on the ISO timescales. The *horizontal axis* represents the meridional distance with respect to maximum convection centre. The *positive* (negative) value means to the north (south) of Convection centre. Here different variables are scaled with different factors for easy scaling

along with the positive Q_{net} (Fig. 12e) that leads to the SST variation at ISO timescales over BoB region as in OBS. However, the surface heat and radiation fluxes along with the surface wind in GFS(d) do not seem to determine the SST variation at all. To summarize the finding, Fig. 13 shows a linear plot of lead-lag relationship among Q_{net}, SST and rainfall, area averaged on the same 5° × 5° box (15°–20°N; 87°–92°E) over BoB region. It confirms that with high frequency interactive SST, CFSv2 shows coherent phase-relationship as in OBS. It is noted that the positive Q_{net} leads the positive SST anomalies that finally drives the convection anomalies ahead. In GFS(d), even though Q_{net} leads SST and rainfall, SST-rainfall relationship is not captured in absence of the air-sea interaction. Thus in the CFSv2, increased shortwave radiation induces surface heating and reduced LHF and that can in turn increase SST and leads to unstable atmosphere and increased convection. But it seems that GFS(d) fails to reproduce the lead-lag relationship between SST and the fluxes that eventually restricts the convection anomalies to move northward. In CFSv2, the SST anomalies are affected by the MISO transformed fluxes and it remains ahead of MISO convection in the region, where oceanic heating is taking place similar to OBS. As the MISO convection adjusts to the new anomaly by its northward propagation, the anomaly itself will propagate further north. In contrast, AGCM fluxes have no impact on the SST and the convection tends to move to the favorable SST (i.e. close to the positive SST anomaly). In the atmosphere-only GFS model, this relationship is stronger as convection and SST coincides.

4 Summary and conclusion

The socio-economical growth in the Indian subcontinent is strongly interlaced with the summer monsoon rainfall associated with the monsoon intraseasonal oscillations (MISO). Therefore, understanding the complex space–time characteristics and northward propagation mechanism of the MISOs, its realistic simulation and prediction have received considerable attention in recent years. Although atmospheric dynamic mechanisms have been prevalently used to explain the characteristics of the MISOs, the significant impact of the ocean–atmosphere interaction in modulating the MISO is still a growing interest. Over the last decade, a large number of observational studies have indicated an active role of SST on the tropical intraseasonal oscillations. A number of recent modeling studies have also explored the same issue and came to a similar conclusion. However, most of these results are model dependent, and concluded that it is the AGCM that produces tropical ISO like oscillation, which is then modified by the inclusion of an interactive SST via coupling. In the present study, we provide a new insight on the dynamics for northward propagation of MISO. We demonstrate that air-sea interaction not only helps in simulating observed amplitude and

periodicity of the MISO, it can also help significantly in producing northward propagation of MISO. We derive this from our attempt to understand the role of basic state and air-sea interaction in the simulation and northward propagation of MISO in both the coupled and atmosphere-only versions of a state-of-the-art model (NCEP CFSv2).

A comparative analysis of CFSv2 and GFS brings out the role of air-sea coupling in the simulation of MISO and its northward movement. The wavenumber-frequency spectra indicates that, though the wavenumbers are similar, the models have slightly higher periodicity (~60 days) compared to observations (~45 days). The power of the

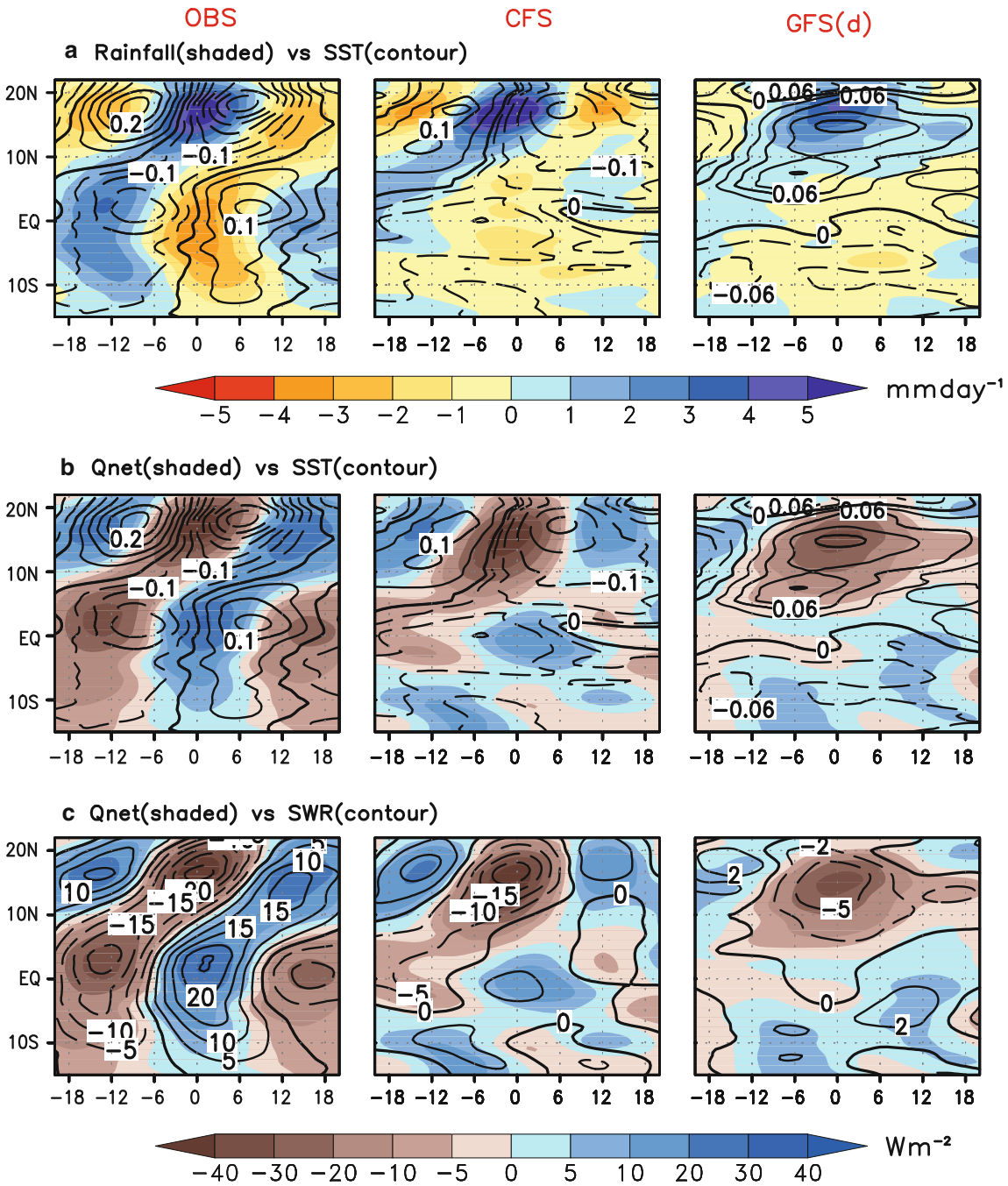

Fig. 12 Time-latitude diagrams of 20–100 day filtered intraseasonal anomalies over Bay of Bengal (BoB) averaged over 85°–95°E for OBS, CFS and GFS(d) shown in column respectively. The lag-lead relation between **a** rainfall (mm day^{-1}) and Sea surface temperature (SST; °C), **b** Net surface heat flux (Q_{net}; Wm^{-2}) and SST, **c** Q_{net} and Shortwave radiation (SWR; Wm^{-2}), **d** rainfall (mm day^{-1}) and zonal wind at 1,000 hPa (U_{1000}; ms^{-1}), **e** surface latent heat flux (LHF; Wm^{-2}) and Q_{net}, **f** LHF and U_{1000} are shown for observation and models in each column. Here day 0 is the day of rainfall maxima

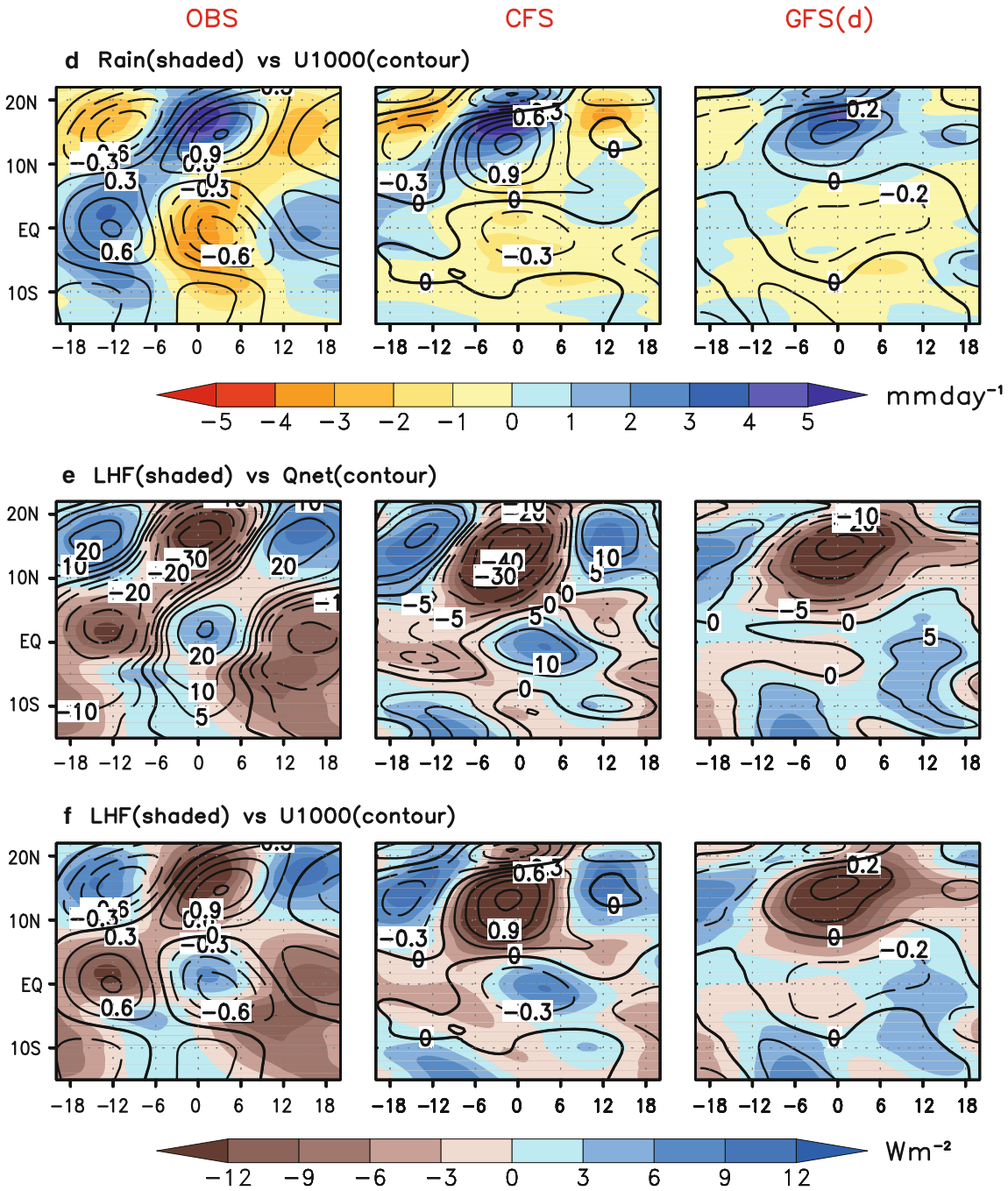

Fig. 12 continued

northward component is low in GFS(m), which slightly improves with GFS(d), whereas in CFSv2 the power is closer to observations. This is expected and has been reported in earlier studies (e.g. Fu et al. 2003). These results confirm that both the AGCM and CGCM have ISO type oscillations. However, the northward propagation indicates that MISO is a standing mode in GFS(m) and has a slightly tilted structure. Thus, even in the presence of realistic vertical wind shear, the absence of adequate moistening of atmosphere in the GFS(d) and GFS(m) ahead of convection, suppressed an active northward propagation of MISO in the AGCM. The absence of northward propagation is related to the lack of strong meridional gradient of the mean moisture field and can be seen in the two band seasonal rainfall structure and in the climatological descent zone of Hadley circulation between 0 and 10°N. The ocean–atmosphere coupling is successful in correcting these errors and significantly reducing the biases in the mean state and the moisture field. This facilitates the propagation of moisture field northward ahead of

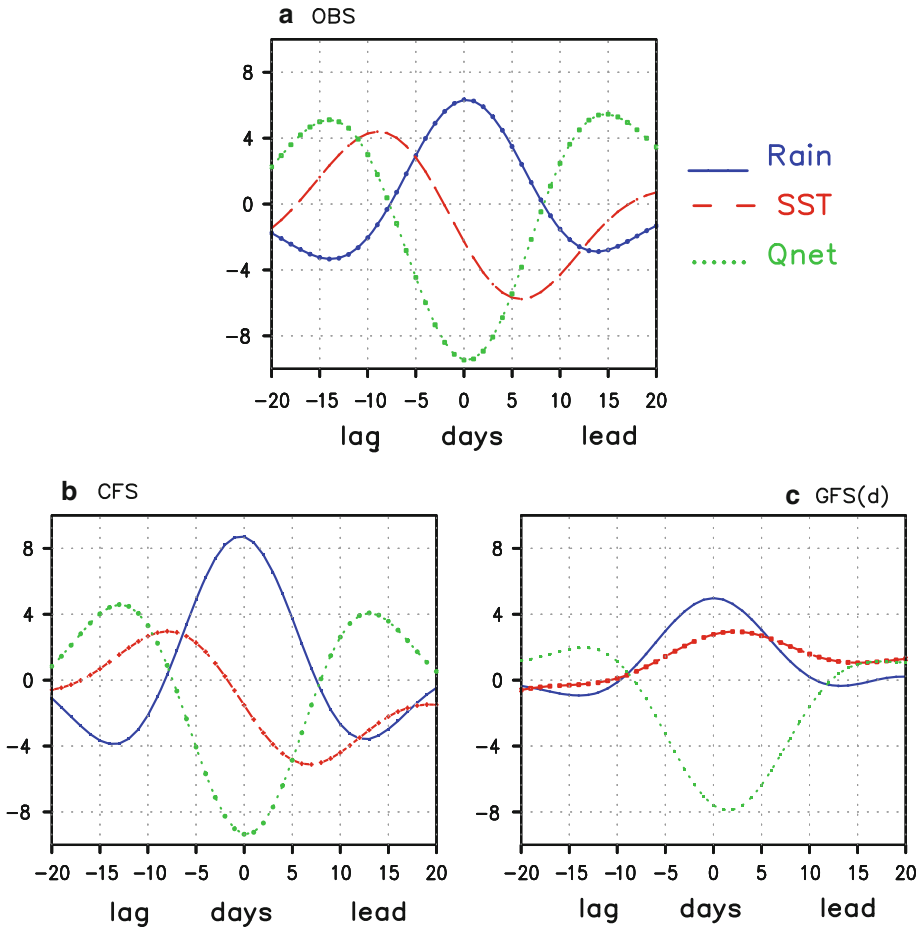

Fig. 13 Lag-lead relationship between rainfall (blue, *solid line*), SST (red, *dash line*) and net surface heat flux (Q_{net}; *green dot line*) on a 5° x 5° box (15°–20°N; 87°–92°E) over Bay of Bengal for **a** OBS and model simulations **b** CFS and **c** GFS(d) respectively. Day 0 is the day of rainfall maxima. Here SST and Q_{net} are scaled with different factors for easy scaling

convection and producing northward propagation of MISO. In particular, air-sea interaction modifies the mean state in such a way in CFSv2 that increased shortwave radiation and reduced LHF induces surface heating, increased SST and leads to unstable atmosphere and increased convection north of the original convection maximum. In GFS(d), however, there is only in situ changes to the fluxes, SST and convection.

In conclusion, the present study suggests that ocean–atmosphere coupling with high frequency interactive SST is a necessary and crucial condition for the reproducing realistic northward propagation of MISO in this particular model. Regardless the issues related to the biases in the model, it is speculated that the performance of coupled version of the CFSv2 model is advantageous for reliable extended range prediction of ISM. Based on this speculation, this model has been used for the extended range prediction of MISO and a detailed hindcast skill analysis will be reported in another paper.

Acknowledgments This work is a part of PhD dissertation of Sharmila S, financially supported by the Council of Scientific and Industrial Research (CSIR), New Delhi, India. The authors thank the Editor and two anonymous reviewers for their valuable comments. Support from NCEP in providing the CFSv2 model, through the National Monsoon Mission is acknowledged. All model runs are carried out on Prithvi IBM High Performance Computing system at Indian Institute of Tropical Meteorology (IITM), Pune India. The authors also wish to thank NCEP-NCAR, USA for the reanalysis datasets, GPCP and IMD for daily gridded rainfall data. NASA/GSFC is thankfully acknowledged for TMI satellite data available at www.remss.com. The surface flux data is obtained from TropFlux Project (http://www.locean-ipsl.upmc.fr/tropflux). The software GRACE and GrADS (COLA) are also acknowledged. IITM is fully supported by Ministry of Earth Sciences (MoES), Govt. of India, New Delhi.

Appendix: Moisture and moist static energy (MSE) budget calculations

Here we provide a brief description of MSE calculation. The vertical integrated temperature (T) and moisture (q) equations for the perturbations have following form:

$$\partial_t\langle T\rangle' + \langle D_T T\rangle' + \langle \omega\partial_p s\rangle' = \langle Q_c\rangle' + \frac{g}{P_T}\left(F'_{rad} + H'\right) \quad (1)$$

$$\partial_t\langle q\rangle' + \langle D_T q\rangle' + \langle \omega\partial_p q\rangle' = \langle Q_q\rangle' + \frac{g}{P_T}\left(E'\right) \quad (2)$$

where both T' and q' are in energy units (W/m^2) after absorbing the heat capacity at constant pressure (C_p) and latent heat of condensation (L) respectively. $s' = T' + \Phi'$ is dry static energy, with Φ' the geopotential. Q_c and Q_q are

anomalous convective heating and moisture sink, respectively. Here, g is acceleration due to gravity, ω is vertical pressure velocity, and P_T is the reference pressure depth of the troposphere. F'_{rad} is the net radiative flux convergence into the atmospheric column. The surface sensible and latent heat fluxes are H' and E', respectively. The second and third term of left side of Eq. (2) represents the horizontal and vertical advection of moisture. The horizontal term can be again split into contribution from zonal and meridional component. The symbol $\langle\rangle$ indicates vertical integration. Combining (1) and (2), the vertically integrated anomalous MSE equation is

$$\left\langle \frac{dh}{dt} \right\rangle' = \langle -V.\nabla h \rangle' - \langle \omega \partial_p h \rangle' + \frac{g}{P_T}\left(F'_{rad} + H' + E'\right)$$

$h = s + q$, is the moist static energy.

References

Abhik S, Halder M, Mukhopadhyay P, Jiang X, Goswami BN (2013) A possible new mechanism for northward propagation of boreal summer intraseasonal oscillations based on TRMM and MERRA reanalysis. Clim Dyn 40:1611–1624

Achuthavarier D, Krishnamurthy V (2011a) Daily modes of South Asian summer monsoon variability in the NCEP Climate Forecast System. Clim Dyn 36:1941–1958. doi:10.1007/s00382-010-0844-9

Achuthavarier D, Krishnamurthy V (2011b) Role of Indian and Pacific SST in Indian summer monsoon intraseasonal variability. J Clim 24:2915–2930

Annamalai H, Slingo JM (2001) Active/break cycles: diagnosis of the intraseasonal variability of the Asian summer monsoon. Clim Dyn 18:85–102

Behringer DW, Xue Y (2004) Evaluation of the global ocean data assimilation system at NCEP: the Pacific Ocean, eighth symposium on integrated observing and assimilation system for atmosphere, ocean, and land surface, AMS 84th annual meeting, 11–15

Bellon G, Sobel AH (2008) Poleward-propagating intraseasonal monsoon disturbances in an intermediate-complexity axisymmetric model. J Atmos Sci 65:470–489

Bhat GS, Vecchi GA, Gadgil S (2004) Sea surface temperature of the Bay of Bengal derived from the TRMM microwave imager. J Atmos Ocean Technol 21:1283–1290

Chaudhari HS, Pokhrel S, Saha SK, Dhakate A, Yadav R, Salunke K, Mahapatra S, Sabeerali C, Rao SA (2013) Model biases in long coupled runs of NCEP CFS in the context of Indian summer monsoon. Int J Climatol 33:1057–1069

Drbohlav HK-L, Wang B (2005) Mechanism of the northward propagating Intraseasonal oscillations: insight from a zonally symmetric model. J Clim 18:952–972

Duchon CE (1979) Lanczos filtering in one and two dimensions. J Appl Meteorol 18:1016–1022

Ek M, Mitchell K, Lin Y, Rogers E, Grunmann P, Koren V, Gayno G, Tarpley J (2003) Implementation of Noah land surface model advances in the National centers for environmental prediction operational mesoscale Eta model. J Geophys Res 108(D22):8851

Fu X, Wang B (2004) The boreal-summer intraseasonal oscillations simulated in a hybrid coupled atmosphere–ocean model. Mon Wea Rev 132:2628–2649

Fu XH, Wang B, Li T, McCreary JP (2003) Coupling between northward-propagating, intraseasonal oscillations and sea surface temperature in the Indian Ocean. J Atmos Sci 60(15):1733–1753

Fu X, Yang B, Bao Q, Wang B (2008) Sea surface temperature feedback extends the predictability of tropical intraseasonal oscillation. Mon Wea Rev 136(2):577–597

Gadgil S, Sajani S (1998) Monsoon precipitation in the AMIP runs. Clim Dyn 14:659–689

Goswami BN (1998) Interannual variation of Indian summer monsoon in a GCM: external conditions versus internal feedbacks. J Clim 11:501–522

Goswami BN (2011) South Asian summer monsoon. In: Lau WK-M, Waliser DE (eds) Intraseasonal variability of the atmosphere-Ocean climate system, 2nd edn. Springer, Berlin, pp 21–72

Goswami BN, Shukla J (1984) Quasi-periodic oscillations in a symmetric general circulation model. J Atmos Sci 41:20–37

Goswami BN, Annamalai H, Krishnamurthy V (1999) A broad scale circulation index for interannual variability of the Indian summer monsoon. Q J R Met Soc 125:611–633

Goswami BN, Ajayamohan RS, Xavier PK, Sengupta D (2003) Clustering of low pressure systems during the Indian summer monsoon by intraseasonal oscillations. Geophys Res Lett 30(8):1431. doi:10.1029/2002GL016734

Goswami BN, Wu G, Yasunari T (2006) Annual cycle, intraseasonal oscillations and roadblock to seasonal predictability of the Asian summer monsoon. J Clim 19:5078–5099

Griffies SM, Harrison MJ, Pacanowski RC, Rosati A (2004) A technical guide to MOM4. GFDL Ocean Group Tech Rep 5:371

Huffman GJ, Adler RF, Bolvin DT, Gu G(2009) Improving the global precipitation record: GPCP version 2.1. Geophys Res Lett 36:L17808. doi:10.1029/2009GL040000

Jiang X, Li T, Wang B (2004) Structures and mechanisms of the northward propagating boreal summer intraseasonal oscillation. J Clim 17:1022–1039

Jiang X, Waliser DE, Li JL, Woods C (2011) Vertical cloud structures of the boreal summer intraseasonal variability based on CloudSat observations and ERA-interim reanalysis. Clim Dyn 36:2219–2232

Joseph S, Sahai AK, Goswami BN, Terray P, Masson S, Luo JJ (2012) Possible role of warm SST bias in the simulation of boreal summer monsoon in SINTEX-F2 coupled model. Clim Dyn 38:1561–1576. doi:10.1007/s00382-011-1264-1

Kalnay E et al (1996) The NCEP/NCAR 40- year reanalysis project. Bull Am Meteorol Soc 77:437–471

Kemball-Cook S, Wang B (2001) Equatorial Waves and Air–Sea interaction in the boreal summer intraseasonal oscillation. J Clim 14:2923–2942

Kemball-Cook S, Wang B, Fu X (2002) Simulation of the ISO in the ECHAM-4 model: the impact of coupling with an ocean model. J Atmos Sci 59:1433–1453

Kim D, Sobel AH, Maloney ED, Dargan M, Frierson W, Kang I (2011) A systematic relationship between intraseasonal variability and mean state bias in AGCM simulations. J Clim 24:5506–5520

Krishnamurti TN, Oosterhof DK, Metha AV (1988) Air–sea interaction on the timescale of 30 to 50 days. J Atmos Sci 45:1304–1322

Lau KM, Peng L (1987) Origin of low-frequency (intraseasonal) oscillations in the tropical atmosphere. Part I: basic theory. J Atmos Sci 44:950–972

Lin J et al (2006) Tropical intraseasonal variability in 14 IPCC AR4 climate models. Part 1: convective signals. J Clim 19:2665–2690

Moorthi S, Pan HL, Caplan P (2001) Changes to the 2001 NCEP operational MRF/AVN global analysis/forecast system. NWS Tech Proced Bull 484:14

Prasanna V, Annamalai H (2012) Moist dynamics of extended monsoon breaks over South Asia. J Clim 25:3810–3831

Praveen Kumar B, Vialard J, Lengaigne M, Murty VSN, McPhaden MJ (2012) TropFlux: air-sea fluxes for the global tropical oceans: description and evaluation. Clim Dyn 38(7–8):1521–1543

Rajeevan M, Nanjundiah RS (2009) Coupled model simulations of twentieth century climate of the Indian summer monsoon, Current Trend in Science, Platinum Jubilee Special, 537–568

Rajeevan M, Bhate J, Kale JD, Lal B (2006) High resolution daily gridded rainfall data for the Indian region: analysis of break and active monsoon spell. Curr Sci 91:296–306

Rajendran K, Kitoh A (2006) Modulation of tropical intraseasonal oscillations by atmosphere–ocean coupling. J Clim 19:366–391

Rajendran K, Nanjundiah RS, Gadgil S, Srinivasan J (2012) How good are the simulations of tropical SST–rainfall relationship by IPCC AR4 atmospheric and coupled models? J Earth Sys Sci 121(3):595–610

Roxy M, Tanimoto Y (2007) Role of SST over the Indian Ocean in influencing the intraseasonal variability of the Indian Summer Monsoon. J Meteoro Soc Jpn 85(3):349–358. doi:10.2151/jmsj.85.349

Roxy M, Tanimoto Y (2012) Influence of sea surface temperature on the intraseasonal variability of the South China Sea summer monsoon. Clim Dyn 39(5):1209–1218. doi:10.1007/s00382-011-1118-x

Roxy M, Tanimoto Y, Preethi B, Pascal T, Krishnan R (2012) Intraseasonal SST-precipitation relationship and its spatial variability over the tropical summer monsoon region. Clim Dyn. doi:10.1007/s00382-012-1547-1

Saha S et al (2006) The NCEP climate forecast system. J Clim 19(15):3483–3517

Saha S et al (2010) The NCEP climate forecast system reanalysis. Bull Am Meteorol Soc 91(8):1015–1057

Saha S et al (2013) The NCEP climate forecast system version 2. J Clim under review. Available at http://cfs.ncep.noaa.gov/cfsv2.info/CFSv2_paper.pdf

Sengupta D, Goswami BN, Senan R (2001) Coherent intraseasonal oscillations of ocean and atmosphere during the Asian summer monsoon. Geophys Res Lett 28(21):4127–4130

Seo KH, Schemm JKE, Wang W, Kumar A (2007) The boreal summer intraseasonal oscillation simulated in the NCEP Climate Forecast System: the effect of sea surface temperature. Mon Wea Rev 135:1807–1827

Sikka DR, Gadgil S (1980) On the maximum cloud zone and the ITCZ over Indian, longitudes during the southwest monsoon. Mon Weather Rev 108:1840–1853

Slingo JM et al (1996) Intraseasonal oscillations in 15 atmospheric general circulation models: results from an AMIP diagnostic subproject. Clim Dyn 12:325–357

Vecchi GA, Harrison DE (2002) Monsoon breaks and subseasonal sea surface temperature variability in the Bay of Bengal. J Clim 15(12):1485–1493

Waliser DE (2006) Intraseasonal variability. In: Wang B (ed) The Asian monsoon, chap 5. Praxis Springer, Chichester, pp 203–258

Waliser DE et al (2003) AGCM simulations of intraseasonal variability associated with the Asian summer monsoon. Clim Dyn 21:423–446. doi:10.1007/s00382-003-0337-1

Waliser DE, Murtugudde R, Lucas L (2004) Indo-Pacific ocean response to atmospheric intraseasonal variability. Part II: boreal summer and the intraseasonal oscillation. J Geophys Res Oceans 109:C03030. doi:10.1029/2003JC002002

Wang B (1988) Dynamics of tropical low-frequency waves: an analysis of the moist kelvin wave. J Atmos Sci 45:2051–2065

Wang B (2005) Theory. In: Lau WK-M, Waliser DE (eds) Intraseasonal variability of the atmosphere ocean climate system. Chapter 10 Springer, Berlin, pp 307–360

Wang B, Xie X (1997) A model for the boreal summer intraseasonal oscillations. J Atmos Sci 54:72–86

Webster PJ (1983) Mechanisms of monsoon low-frequency variability: surface hydrological effects. J Atmos Sci 40:2110–2124

Webster PJ, Magana VO, Palmer TN, Shukla J, Thomas RA, Yani M, Yasunari T (1998) The monsoon: processes, predictability and prediction. J Geophys Res 103:14451–14510

Webster PJ et al (2002) The JASMINE pilot study. Bull Am Meteor Soc 83:1603–1629

Wheeler M, Kiladis GN (1999) Convectively coupled equatorial waves: analysis of clouds and temperature in the wave number frequency domain. J Atmos Sci 56:374–399

Wu R (2010) Subseasonal variability during the South China Sea summer monsoon onset. Clim Dyn 34(5):629–642

Wu MLC, Schubert S, Kang IS, Waliser DE (2002) Forced and free intraseasonal variability over the South Asian monsoon region simulated by 10 AGCMs. J Clim 15:2862–2880

Wu R, Kirtman BP, Pegion K (2008) Local rainfall-SST relationship on subseasonal time scales in satellite observations and CFS. Geophys Res Lett 35(22):L22706. doi:10.1029/2008gl035883

Xavier PK, Duvel JP, Doblas-Reyes FJ (2008) Boreal summer intraseasonal variability in coupled seasonal hindcasts. J Clim 21(17):4477–4497

Yasunari T (1979) Cloudiness fluctuation associated with the northern hemisphere summer monsoon. J Met Soc Jpn 57:227–242

Yasunari T (1980) A quasi-stationary appearance of the 30–40 day period in the cloudiness fluctuations during the summer monsoon over India. J Met Soc Jpn 58:225–229

Yu L, Jin X, Weller RA (2008) Multidecade global flux datasets from the objectively analyzed air-sea fluxes (OAFlux) project: latent and sensible heat fluxes, ocean evaporation, and related surface meteorological variables. Woods Hole Oceanographic Institution, OAFlux Project Technical Report. OA-2008-01, 64 pp